

# Bulk Nd<sup>3+</sup>-doped tellurite glass laser at 1.37 μm

H. Cankaya · A. Sennaroglu

Received: 22 July 2009 / Revised version: 28 August 2009 / Published online: 2 October 2009  
© Springer-Verlag 2009

**Abstract** We have demonstrated, for the first time to our knowledge, lasing at 1.37 μm in a tellurite-based glass host doped with 0.5 mol.% neodymium: Nd<sup>3+):(0.8)TeO<sub>2</sub>–(0.2)WO<sub>3</sub>. The gain-switched laser could be operated with 59 μJ threshold pulse energy as well as 5.5% slope efficiency. As high as 6 μJ-pulses with a duration of 1.74 μs were obtained. The pulse repetition rate was 1 kHz. The emission cross section from the threshold analysis turned out to be  $1.57 \times 10^{-20} \text{ cm}^2$  at 1370 nm by taking into account excited-state absorption from  ${}^4\text{F}_{3/2}$  to  ${}^4\text{G}_{7/2}$  energy level. Furthermore, the ratio of excited-state absorption to the emission cross section was found out to be 0.78 by using the slope efficiency value.</sup>

**PACS** 42.55.Rz · 42.70.Ce · 42.70.Hj · 42.72.Ai · 42.60.Lh

## 1 Introduction

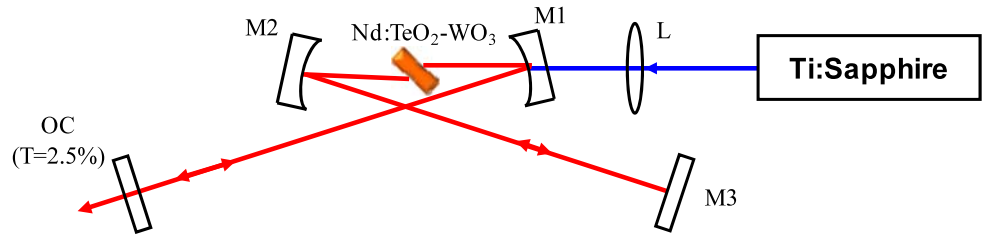
There is a growing demand for coherent light sources operating in the 1.3–1.4 μm window for biomedical imaging applications [1, 2]. In comparison with more widely used sources at 800 nm and 1 μm, use of higher wavelength lasers significantly decreases the losses due to Rayleigh scattering and enables deeper tissue penetration. Furthermore, staying below 1.4 μm avoids water absorption losses. As potential laser hosts, glasses offer several advantages over single crystals, including far lower cost, simpler preparation techniques, and the possibility of power scaling when drawn

into fiber. Due to these advantages, there have been many studies aimed at the development of glass lasers doped with rare-earth ions. In the particular case of neodymium (Nd<sup>3+</sup>)-doped systems, lasing has been reported in various glass matrices including fluorides [3, 4], chalcogenides [5], aluminosilicates [6], germinates [7], and tellurites [8–11]. Among these, tellurite-based glasses have attractive properties including a wide transparency range (0.35–5.0 μm), a high refractive index, lower non-radiative decay rates than silicates, phosphates or germanates, and resistance to corrosion [12–14]. In addition, tellurite-based glasses are considered to be strong candidates as laser host materials because they have the highest emission cross section among the Nd<sup>3+</sup>-doped oxide glasses [12]. To date, lasing could be obtained from a bulk tellurite glass from the  ${}^4\text{F}_{3/2} \rightarrow {}^4\text{I}_{11/2}$  transition of the Nd<sup>3+</sup> ion [8–11] which corresponds to the wavelength of around 1064 nm. However, the lasing operation has not been achieved so far for the  ${}^4\text{F}_{3/2} \rightarrow {}^4\text{I}_{13/2}$  transition, which generates radiation in the 1.34–1.37 μm spectral region.

In this letter, we report for the first time to our knowledge, lasing action at 1370 nm from  ${}^4\text{F}_{3/2} \rightarrow {}^4\text{I}_{13/2}$  transition of Nd<sup>3+</sup> ion in a bulk tellurite glass host where the emission cross section is lower than that for the  ${}^4\text{F}_{3/2} \rightarrow {}^4\text{I}_{11/2}$  transition. The glass sample had a composition of (0.8)TeO<sub>2</sub>–(0.2)WO<sub>3</sub> with 0.5 mol.% Nd<sub>2</sub>O<sub>3</sub>. The laser could be operated in gain-switched regime at 1 kHz with as low as 59 μJ of threshold pulse energy. In addition, the slope efficiency was determined to be 5.5%. As a pump source, we used a pulsed Ti:sapphire laser at the wavelength of 805 nm. From the analysis of threshold data, we determined the emission cross section to be  $1.57 \times 10^{-20} \text{ cm}^2$  at the wavelength of 1370 nm. Lasing could not be obtained over the broad emission band, believed to be due to excited-state absorption. By using the lasing efficiency data, we further esti-

H. Cankaya · A. Sennaroglu (✉)  
Laser Research Laboratory, Department of Physics,  
Koç University, Rumelifeneri, Sarıyer, 34450 Istanbul, Turkey  
e-mail: [asennar@ku.edu.tr](mailto:asennar@ku.edu.tr)

**Fig. 1** Schematic of the gain-switched, bulk neodymium-doped tellurite ( $\text{Nd}^{3+}:\text{TeO}_2-\text{WO}_3$ ) glass laser



mated the excited-state absorption cross section  $\sigma_{\text{ESA}}$  to be  $1.22 \times 10^{-20} \text{ cm}^2$ . The ratio of the excited-state and stimulated emission cross sections (0.78) is consistent with the reported value obtained for  $\text{SiO}_2$ -based Nd:glass fiber operating at  $1.36 \mu\text{m}$  [15].

## 2 Experimental

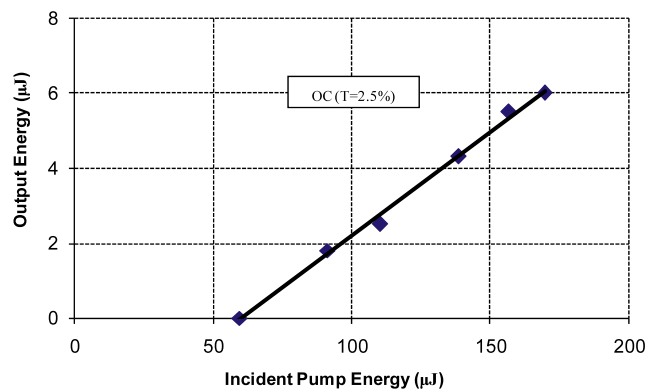
The tellurite glass sample was prepared with the composition of  $\text{Nd}^{3+} : (0.8)\text{TeO}_2-(0.2)\text{WO}_3$  by melting powder mixtures of  $\text{Nd}_2\text{O}_3$  (99.9% purity),  $\text{TeO}_2$  (99.999% purity), and  $\text{WO}_3$  (99% purity). The batch containing 0.5 mole of  $\text{Nd}_2\text{O}_3$  to 100 moles of  $(0.8)\text{TeO}_2-(0.2)\text{WO}_3$  was mixed and melted in a platinum crucible at  $800^\circ\text{C}$  for 1 hour in an electrically heated furnace in ambient air atmosphere. Then, the glass melt was rapidly quenched in a preheated stainless steel mold at the temperature around  $150^\circ\text{C}$ . To release the residual thermal stresses formed in the glass during the quenching process, the sample was annealed below the glass transition temperature at  $250^\circ\text{C}$ . Sample surfaces were then polished to a thickness of 4.1 mm. Using the measured density of  $5.82 \text{ gm/cm}^3$ , the  $\text{Nd}^{3+}$  ion concentration was determined to be  $2.02 \times 10^{20} \text{ cm}^{-3}$ . The single-pass absorption at the pump wavelength of  $805 \text{ nm}$  was 92%.

Figure 1 shows a schematic of the standard astigmatically compensated x-cavity laser setup. The cavity consisted of two curved highly reflecting mirrors with radius of curvature 5 cm (M1 and M2), a flat end high reflector (M3), and a flat output coupler with transmission of 2.5% at  $1370 \text{ nm}$  (OC). The highly reflecting mirrors have reflectivity above 99.9% in the range of  $1150$ – $1450 \text{ nm}$  and transitivity above 90% at  $1065 \text{ nm}$ , which prevents laser operation at that wavelength. As a pump source, we used a home-made, tunable, pulsed Ti:sapphire laser at  $805 \text{ nm}$  with a pulse repetition rate of 1 kHz. The output of the pump laser was focused inside the glass sample by using a lens with a focal length of 5 cm. The pump beam waist was measured to be  $27 \mu\text{m}$  with the knife-edge technique. The high reflector and output coupler arm lengths were 31 and 32 cm, respectively, giving an estimated beam waist of  $21 \mu\text{m}$  near the middle of the stability range. The time-dependent fluorescence signal and pulse traces of glass and pump lasers were measured with a digital oscilloscope and a Ge PIN detector (response time

of 3.5 ns). Emission spectrum and wavelength measurements were performed with a 1/2-m Czerny-Turner-type monochromator and a PbS detector coupled with a lock-in amplifier.

## 3 Results and discussion

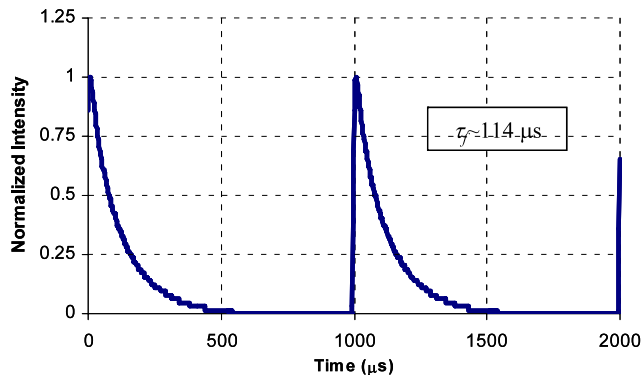
The power efficiency curve of the  $\text{Nd}^{3+}$ :tellurite glass laser operating at  $1370 \text{ nm}$  is shown in Fig. 2. The slope efficiency of the laser was determined to be 5.5% with respect to the incident pump pulse energy. The laser could be operated with as low as  $59 \mu\text{J}$  of incident threshold pulse energy and we obtained as high as  $6 \mu\text{J}$  of output pulse energy. To determine the passive loss of the resonator, the threshold pump power of the laser was also measured by replacing the output coupler with a flat high reflecting mirror. The corresponding threshold energy decreased to  $32 \mu\text{J}$ . By comparing the threshold pulse energy for two different output coupling levels, we determined the round trip passive loss of the cavity ( $L$ ) to be 2.9%. Here, we assumed that the threshold pump energy is directly proportional to  $(L + T)$  where  $T$  is the output coupling level. Furthermore, the optimum output coupling level can be found by using the formula,  $T_{\text{opt}} = L(\sqrt{r} - 1)$ , where  $r$  is the ratio of maximum available pump pulse energy to the threshold pulse energy ( $r = E_p/E_{\text{th}}$ ) for zero output coupling (32  $\mu\text{J}$ ). In our case, the optimum output coupler level turned out to be about



**Fig. 2** Energy efficiency curve of  $\text{Nd}^{3+}$ :tellurite glass laser. The slope efficiency is around 5.5%. The transmission of the output coupler (OC) is 2.5% at  $1370 \text{ nm}$

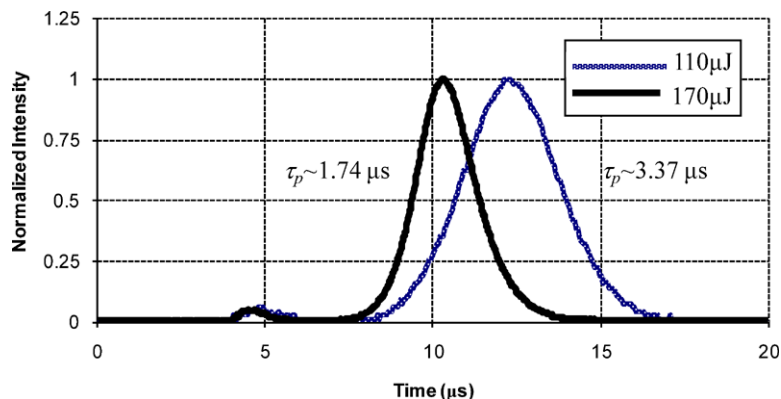
3.8% at the maximum available pump energy of 169 μJ. The corresponding estimated output energy for optimum output coupling becomes 6.5 μJ, which is close to experimentally obtained pulse energy with the 2.5% output coupler.

Figure 3 shows the time-dependent fluorescence decay curve for the  $^4F_{3/2} \rightarrow ^4I_{13/2}$  transition. From the decay data, the fluorescence lifetime was determined to be 114 μs. In our previous study about 1065 nm laser action of the same host,

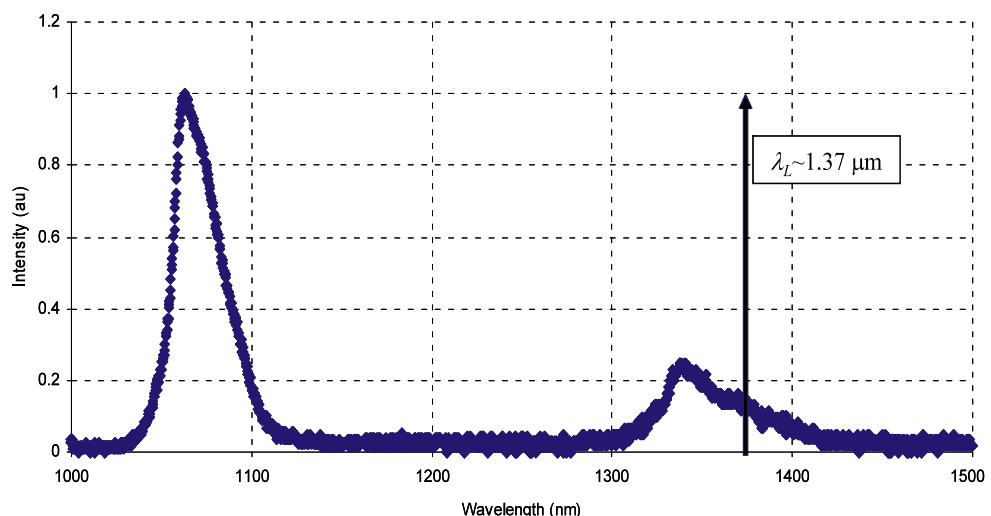


**Fig. 3** Fluorescence decay curves for the Nd<sup>3+</sup>:tellurite glass sample at 1.37 μm. The fluorescence lifetime is around 114 μs

**Fig. 4** Temporal profiles of the laser pulses at a pump energy of 110 and 170 μJ



**Fig. 5** Emission spectrum of the Nd<sup>3+</sup>:tellurite glass sample in the 1000–1500 nm range. The laser was operating at 1.37 μm



the fluorescence lifetime for the  $^4F_{3/2} \rightarrow ^4I_{11/2}$  transition was measured to be 142 μs [11] which is close to what we had for the  $^4F_{3/2} \rightarrow ^4I_{13/2}$  transition, as expected. Furthermore, Fig. 4 shows the temporal profile of the output laser pulses at different pump energies. As can be seen, the output pulse width drops from 3.37 to 1.74 μs as the pump pulse energy increases from 110 to 170 μJ. In this pumping level range, the pump pulse width remains almost constant around 116 ns. In Fig. 4, the lower peaks preceding the laser pulses were the pump laser pulses which could not be completely eliminated by the filter. The delay between the pump and laser pulses depended on the pumping level as expected and decreased from 7.4 to 5.6 μs as the incident pump energy was increased from 110 to 170 μJ.

Figure 5 shows the emission spectrum of the glass sample and laser emission. As can be seen from the spectrum, there are two peaks around 1065 and 1342 nm, which correspond to the transitions  $^4F_{3/2} \rightarrow ^4I_{11/2}$  and  $^4F_{3/2} \rightarrow ^4I_{13/2}$ , respectively. From the spectrum measurements, one would expect to get lasing at the peak wavelength of 1342 nm. However, previous studies show that there is a competing excited-state absorption (ESA) at the peak emission wavelength [15–17]. As can be seen from the energy level diagram of Nd<sup>3+</sup>

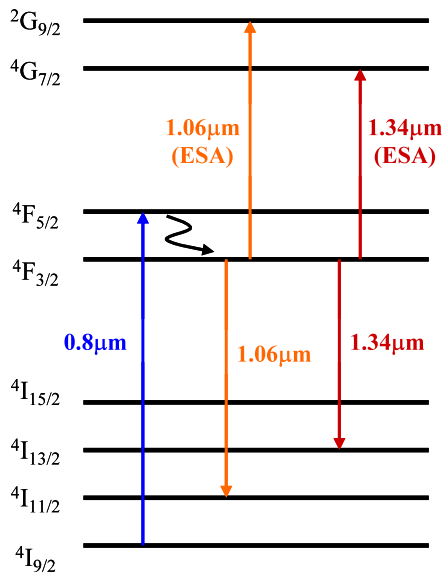


**Fig. 6** Schematic of the partial energy level diagram for the Nd<sup>3+</sup> ion, showing the laser and excited-state absorption transitions

ion (Fig. 6), there are two excited-state absorption transitions  ${}^4F_{3/2} \rightarrow {}^2G_{9/2}$  and  ${}^4F_{3/2} \rightarrow {}^4G_{7/2}$  which correspond to the wavelengths around 1 μm and 1.34 μm, respectively. The transition  ${}^4F_{3/2} \rightarrow {}^2G_{9/2}$  does not introduce any significant loss at 1065 nm laser operation, even though it is close to the lasing wavelength [4]. However, ESA due to  ${}^4F_{3/2} \rightarrow {}^4G_{7/2}$  transition introduces extra loss near the peak of the 1342-nm emission and shifts the laser wavelength to 1.37 μm. To check whether the ambient humidity has any effect on the emission wavelength, we further purged the whole resonator with pure N<sub>2</sub> gas and lowered the relative humidity level from 50 to 12%. No observable change was recorded in the lasing wavelength or the output power of the laser.

The slope efficiency of the laser was used to estimate the ratio of ESA cross section ( $\sigma_{\text{ESA}}$ ) to the emission cross section ( $\sigma_L$ ), ( $f_L = \sigma_{\text{ESA}}/\sigma_L$ ). By assuming that the pump and laser beams are nearly matched inside the gain medium,  $f_L$  can be estimated from [18],

$$\eta = \frac{T}{(T+L)} \frac{\lambda_p}{\lambda_L} \eta_a (1 - f_L). \quad (1)$$

Here,  $\eta$  is the slope efficiency of the laser,  $\eta_a$  is the absorption at the pump wavelength, and  $\lambda_p$  and  $\lambda_L$  are the wavelengths of the pump and the laser beams, respectively. For our case, we estimated  $f_L$  to be 0.78, which is in very good agreement with the reported value for Nd:SiO<sub>2</sub> glass fiber operating at 1.36 μm (0.78) [15]. In addition, we determined the emission cross section ( $\sigma_L$ ) at 1.37 μm from the threshold pulse energy value by taking ESA into account. Under the approximation that the pump pulse width is shorter than

the fluorescence lifetime, the emission cross section can be determined by using the formula [18],

$$\sigma_L = \frac{\pi h v_p (w_L^2 + w_p^2)(T + L)}{4\eta_a E_{\text{th}}(1 - f_L)}, \quad (2)$$

where  $E_{\text{th}}$  is the threshold pulse energy,  $v_p$  is pump photon frequency,  $h$  is the Planck constant,  $w_L$  and  $w_p$  are the laser and pump spot sizes inside the gain medium, respectively. Since the spotsize function varies within the gain medium due to diffractive spreading, we approximated  $w_L$  and  $w_p$  in (2) by their root-mean-squared (rms) values, which turned out to  $w_L = 24 \mu\text{m}$  and  $w_p = 35 \mu\text{m}$ , respectively. If  $w(z)$  is the spot size function of one of the beams, the corresponding rms value  $w_{\text{rms}}$  is calculated by using

$$w_{\text{rms}} = \sqrt{\frac{1}{L_0} \int_0^{L_0} w^2(z) dz}. \quad (3)$$

Here  $L_0$  is the length of the glass. With  $E_{\text{th}} = 32 \mu\text{J}$ ,  $T = 0$  (for the high reflector),  $L = 0.029$ ,  $\eta_a = 0.92$ , the emission cross section,  $\sigma_L$ , was determined to be  $1.57 \times 10^{-20} \text{ cm}^2$  at 1.37 μm. Moreover, by using the calculated  $f_L$  value, the excited-state absorption cross section was estimated to be  $1.22 \times 10^{-20} \text{ cm}^2$  at the wavelength of 1.37 μm.

#### 4 Conclusions

In conclusion, we have reported, for the first time to our knowledge, lasing action at 1370 nm in a bulk tellurite glass from the energy transition  ${}^4F_{3/2} \rightarrow {}^4I_{13/2}$  of the Nd<sup>3+</sup> ion. The laser was operated in gain-switched regime at 1 kHz with a threshold pulse energy of 59 μJ. The slope efficiency was further determined to be 5.5%. As high as 6 μJ-pulses with a duration of 1.74 μs were obtained. From the threshold analysis, the emission cross section turned out to be  $1.57 \times 10^{-20} \text{ cm}^2$  in the presence of excited-state absorption. In addition, the excited-state absorption cross section,  $\sigma_{\text{ESA}}$  was estimated to be  $1.22 \times 10^{-20} \text{ cm}^2$  by using the slope efficiency analysis. The ratio of excited-state to stimulated emission cross section is consistent with the value reported in the literature [15]. The performance of the Nd<sup>3+</sup>-doped tellurite glass laser was limited by excited-state absorption. However, the tellurite glass host is still promising when doped with other ions such as Pr<sup>3+</sup>, which has optical transitions in the same spectral region and is less susceptible to excited-state absorption. Hence, it should be possible to develop efficient near infrared laser systems based on tellurite glass host.

**Acknowledgements** The authors would like to thank Gonul Ozen and M. Lutfu Ovecoglu for their technical support in the preparation of the glass samples and Refik Kortan for providing some of the equipment used in the experiments. A. Sennaroglu further acknowledges the support provided by the Turkish Academy of Sciences.

## References

1. B.E. Bouma, G.J. Tearney, I.P. Bilinsky, B. Golubovic, J.G. Fujimoto, Opt. Lett. **21**, 1839–1841 (1996)
2. G.J. Tearney, M.E. Brezinski, B.E. Bouma, S.A. Boppart, C. Pitriss, J.F. Southern, J.G. Fujimoto, Science **276**, 2037–2039 (1997)
3. R.R. Petrin, M.L. Kliewer, J.T. Beasley, R.C. Powell, I.D. Aggarwal, R.C. Ginther, IEEE J. Quantum Electron. **27**, 1031–1038 (1991)
4. A.S.S. De Camargo, C. Jacinto, T. Catunda, L.A.O. Nunes, Appl. Phys. B **83**, 565–569 (2006)
5. T. Schweizer, D.W. Hewak, D.N. Payne, T. Jensen, G. Huber, Electron. Lett. **32**, 666–667 (1996)
6. D.F. De Sousa, L.A.O. Nunes, J.H. Rohling, M.L. Baesso, Appl. Phys. B **77**, 59–63 (2003)
7. J. Fernandez, I. Iparraguirre, R. Balda, J. Azkargorta, M. Voda, J.M. Fernandez-Navarro, Opt. Mater. **25**, 185–191 (2004)
8. J.C. Michel, D. Morin, F. Auzel, Rev. Phys. Appl. **13**, 859–866 (1978)
9. N. Lei, B. Xu, Z.H. Jiang, Opt. Commun. **127**, 263–265 (1996)
10. I. Iparraguirre, J. Azkargorta, J.M. Fernandez-Navarro, M. Al-Saleh, J. Fernandez, R. Balda, J. Non-Cryst. Solids **353**, 990–992 (2007)
11. H. Kalaycioglu, H. Cankaya, G. Ozen, L. Ovecoglu, A. Sennaroglu, Opt. Commun. **281**, 6056–6060 (2008)
12. M.J. Weber, J.D. Myers, D.H. Blackburn, J. Appl. Phys. **52**, 2944–2949 (1981)
13. J.S. Wang, E.M. Vogel, E. Snitzer, Opt. Mater. **3**, 187–203 (1994)
14. B. Richards, Y. Tsang, D. Binks, J. Lousteau, A. Jha, Opt. Lett. **33**, 402–404 (2008)
15. F. Hakimi, H. Po, R. Tumminelli, B.C. Mccollum, L. Zenteno, N.M. Cho, E. Snitzer, Opt. Lett. **14**, 1060–1061 (1989)
16. M. Brierley, S. Carter, P. France, J.E. Pedersen, Electron. Lett. **26**, 329–330 (1990)
17. W.J. Miniscalco, L.J. Andrews, B.A. Thompson, R.S. Quimby, L.J.B. Vacha, M.G. Drexhage, Electron. Lett. **24**, 28–29 (1988)
18. A. Sennaroglu, C.R. Pollock, H. Nathel, J. Opt. Soc. Am. B **12**, 930–937 (1995)